Figure S1

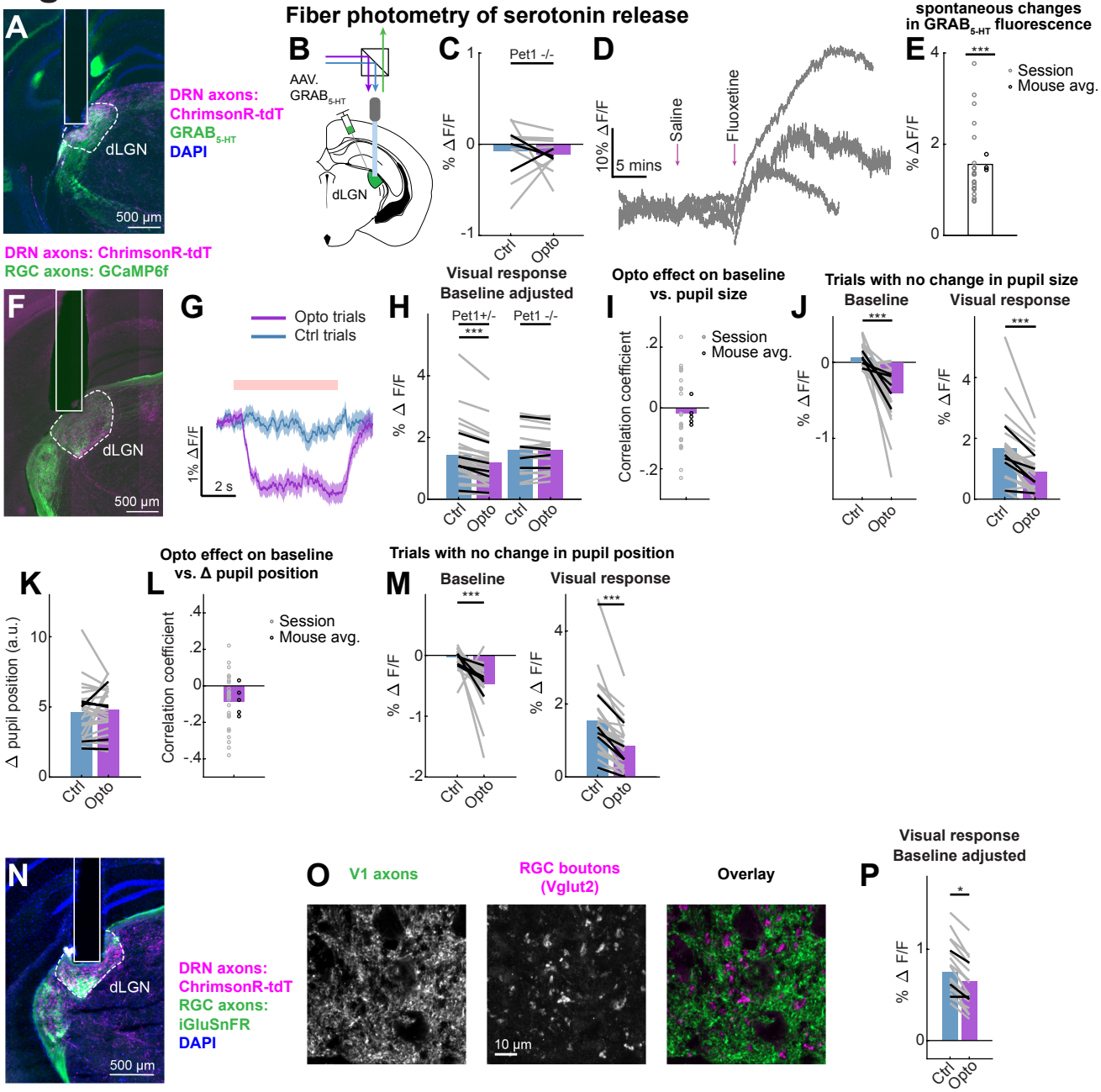
A
dLGN
500 µm
DRN axons:
ChrimsonR-tdT
GRAB5-HT
DAPI
Fiber photometry of serotonin release
B
AAV.
GRAB5-HT
dLGN
C
Pet1 -/-
% ΔF/F
Ctrl
Opto
D
10% ΔF/F
5 mins
Saline
Fluoxetine
E
Std. dev. of
spontaneous changes
in GRAB5-HT fluorescence
Session
Mouse avg.
% ΔF/F
DRN axons: ChrimsonR-tdT
RGC axons: GCaMP6f
F
dLGN
500 µm
G
Opto trials
Ctrl trials
1% ΔF/F
2 s
H
Visual response
Baseline adjusted
Pet1+/-
Pet1 -/-
% Δ F/F
I
Opto effect on baseline
vs. pupil size
Correlation coefficient
Session
Mouse avg.
J
Trials with no change in pupil size
Baseline
Visual response
% ΔF/F
K
Δ pupil position (a.u.)
L
Opto effect on baseline
vs. Δ pupil position
Correlation coefficient
Session
Mouse avg.
M
Trials with no change in pupil position
Baseline
Visual response
% Δ F/F
N
dLGN
500 µm
DRN axons:
ChrimsonR-tdT
RGC axons:
iGluSnFR
DAPI
O
V1 axons
RGC boutons
(Vglut2)
Overlay
10 µm
P
Visual response
Baseline adjusted
% Δ F/F

Figure S1, Fiber photometry recordings from retinal axons in dLGN. Related to Figure 1.

A. Example histology showing $GRAB_{5\text{-}HT}$ expression, DRN innervation (axons expressing ChrimsonR-tdTomato) and fiber placement in dLGN.
B. Experimental set-up in awake head-fixed mice for fiber photometry recordings of $GRAB_{5\text{-}HT}$ expressed in dLGN.
C. Mean percent change in $GRAB_{5\text{-}HT}$ fluorescence on $DRN^{5HT \rightarrow dLGN}$ stimulation ('Opto') and control ('Ctrl') trials in Pet1-$Cre^{-/-}$ mice (8 sessions [gray lines], 3 mice [black lines]). Linear mixed effects model (LME): p = .77.
D. Recordings of $GRAB_{5\text{-}HT}$ fluorescence during i.p. administration of isotonic saline (100 μl) and fluoxetine (100 μl; 16 mg/kg; 3 mice).
E. Standard deviation of spontaneous fluctuations in $GRAB_{5\text{-}HT}$ fluorescence after bleach correction and correcting for motion and other artifacts using concurrent traces with excitation at 405 nm (18 sessions, 3 mice). See also Figure 5 and S5, below and Methods. *** p < .001, linear mixed effects model (LME).
F. Example histology showing GCaMP6f-expressing RGC axons, DRN innervation (axons expressing ChrimsonR-tdTomato) and fiber placement in dLGN.
G. Example trace of calcium activity with (purple, 'Opto' trials) and without (blue, 'Ctrl' trials) $DRN^{5HT \rightarrow dLGN}$ stimulation at baseline (gray screen with no visual stimulation). Red bar indicates time of optogenetic stimulation. Error bars: mean +/- SEM across trials.
H. Mean amplitude of visually evoked calcium responses on Opto and Ctrl trials in Pet1-$Cre^{+/-}$ mice (*left*; 27 sessions, 5 mice), and Pet1-$Cre^{-/-}$ mice (*right*; 16 sessions, 4 mice). The visual response amplitude was measured as the change in fluorescence from the 1 s before visual stimulation onset (i.e. 2 s after the onset of optogenetic stimulation) to the 2 s during the presentation of the visual stimulus. Gray lines: sessions. Black lines: mean per mouse across sessions. LME: ***p<0.001, Pet1-$Cre^{-/-}$: p = 0.73.
I. Correlation coefficient estimating across-trial covariation between arousal state (mean pupil area in the 2 s preceding optogenetic stimulation) and change in baseline fluorescence calculated between the mean of the 2 s before and 2-4 s after optogenetic stimulation on individual trials (24 sessions [gray dots], 5 mice [black dots]; on trials with visual stimulation the change in fluorescence was measure between the mean of 2 s before and 2-3 s after optogenetic stimulation). Positive correlation coefficients: larger pre-stimulation pupil size is correlated with larger suppression. 2/24 coefficients were significant. Additionally, when looking at the correlation between change in baseline fluorescence and change in pupil area from before to during each trial (one correlation coefficient per session), we found these to be mildly inversely correlated on both control and optogenetic stimulation trials (2/24 and 7/24 coefficients were significant, p<0.05).
J. Mean calcium activity at baseline (*left*, mean luminance gray screen) and visually evoked calcium responses (*right*, $\Delta F/F_0$, F_0 estimated during the 2 s before optogenetic stimulation), using only those Opto and Ctrl trials in which pupil area during optogenetic stimulation did not change by more than 1 standard deviation of the pupil area in the 2 s before trial onset. See Fig 1H-I for a similar analysis but using all trials. 24 sessions [gray lines], 5 mice [black lines]). LME: ***p<0.001.
K. Mean change in pupil position on Opto and Ctrl trials, calculated as the Euclidean distance between the position of the pupil center of mass in the 2 s before trials onset to the 2-4 s after optogenetic stimulation (in arbitrary units (a.u.), 24 sessions [gray lines], 5 mice [black lines]; on trials with visual stimulation the change in fluorescence was measure between the mean of 2 s before and 2-3 s after optogenetic stimulation). LME: p = 0.56. See Methods for details.
L. Correlation coefficient between the change in pupil position (see K, and Methods) and the amplitude of the change in baseline fluorescence from 2 s before to 2-4 s after optogenetic stimulation on individual trials (24 sessions [gray dots], 5 mice [black dots]; on trials with visual stimulation the change in fluorescence was measure between the mean of 2 s before and 2-3 s after optogenetic stimulation). Positive correlations coefficients: larger changes in pupil position are correlated with larger suppression. 3/24 coefficients were significant (p<0.05).
M. Mean calcium activity at baseline (*left*, mean luminance gray screen) and visually evoked calcium responses (*right*, $\Delta F/F_0$, F_0 = 2 s before optogenetic stimulation) on Opto and Ctrl trials in which the pupil did not move throughout the duration of the trial (i.e. less than 1 standard deviation in change in pupil position, see Methods). See Fig 1H-I for a similar analysis but using all trials. Gray lines: sessions. Black lines: mean per mouse across sessions. (24 sessions, 5 mice) LME: **p<0.01, ***p<0.001.
N. Example histology showing iGluSnFR-expressing RGC axons, DRN innervation (axons expressing ChrimsonR-tdTomato) and fiber placement in dLGN.

O. Coronal image of mouse dLGN with YFP expressed in V1 corticothalamic axons, and stained for Vglut2 (to label RGC axon terminals) to illustrate the spatial segregation between cortical and retinal inputs to the dLGN.
P. Mean amplitude of visually evoked glutamate release on Opto and Ctrl trials in Pet1-Cre$^{+/-}$ mice (*left*; 18 sessions, 3 mice). The visual response amplitude was measured as the change in fluorescence from the 1 s before visual stimulation onset (i.e. 2 s after the onset of optogenetic stimulation) to the 2 s during the presentation of the visual stimulus. Gray lines: sessions. Black lines: mean per mouse across sessions. LME: *$p<0.05$.

Figure S2

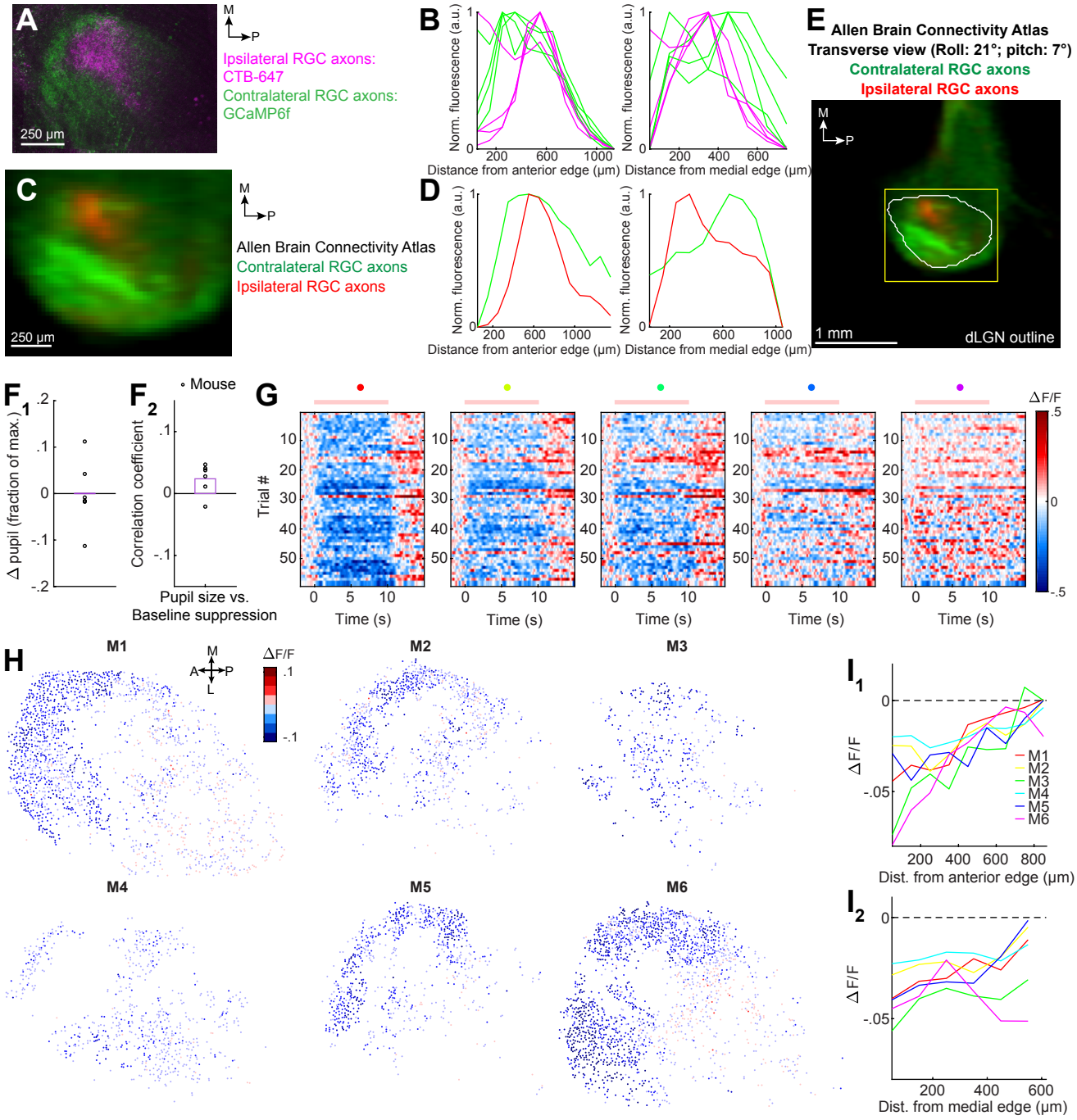
A
M
P
Ipsilateral RGC axons:
CTB-647
Contralateral RGC axons:
GCaMP6f
250 µm
B
Norm. fluorescence (a.u.)
Distance from anterior edge (µm)
Distance from medial edge (µm)
C
Allen Brain Connectivity Atlas
Contralateral RGC axons
Ipsilateral RGC axons
250 µm
D
E
Allen Brain Connectivity Atlas
Transverse view (Roll: 21°; pitch: 7°)
Contralateral RGC axons
Ipsilateral RGC axons
1 mm
dLGN outline
F1
Δ pupil (fraction of max.)
F2
Mouse
Correlation coefficient
Pupil size vs.
Baseline suppression
G
Trial #
Time (s)
ΔF/F
H
M1
M2
M3
M4
M5
M6
A
L
I1
I2
ΔF/F
Dist. from anterior edge (µm)
Dist. from medial edge (µm)

Figure S2, Two-photon calcium imaging of $DRN^{5HT \rightarrow dLGN}$- stimulation-evoked suppression of baseline activity in RGC boutons. Related to Figure 2.

A. Mean image of GCaMP-expressing contralateral RGC axons and CTB-A647 labeled ipsilateral RGC axons in our imaging FOV in dLGN (mean across 4 mice, after alignment of FOVs based on morphology of the GCaMP expression pattern).
B. Quantification of the intensity of CTB-A647 and GCaMP along the anterior-posterior (A-P) and medial-lateral (M-L) axes in the 4 FOVs whose mean image is shown in A. We observed a consistent location of the 'ipsilateral patch' (area of the dLGN innervated by ipsilateral RGC axons) in the anterior-medial area of our FOV.

C-E. Analysis of data from the Allen Mouse Brain Connectivity Atlas (projection pattern of RGCs of different mouse lines labeled using injection of a Cre-dependent fluorescent protein in one eye). The volume of the dLGN was tilted (a tilt in pitch [7°] and roll [21°] was applied to match the angle of the imaging window) and digitally re-sectioned to mimic the view through the cannula during two-photon imaging. Panel C and E were created by superimposing the projections of all RGCs (labeled using Vglut2-Cre) from the contralateral eye (green) with an estimate of input from the ipsilateral eye (red) which we obtained by flipping the 3D volume of the Vglut2-Cre projections along the midline of the brain.

C. The ipsilateral patch (red) is visible and is in a similar region as in our *in vivo* imaging FOVs (panel A). The image is averaged across unilateral intraocular injections in 3 Vglut2-Cre animals, from the Allen Mouse Brain Connectivity Atlas.
D. Quantification of the intensity of contralateral and ipsilateral RGC axons along the A-P and M-L axes in the image in C. We observe a comparable localization of the 'ipsilateral patch' as in our imaging FOV (panel A-B).
E. Lower-magnification view of the same image as in C, zoomed-out to mimic the size of our 3-mm diameter imaging cannula. This illustrates that in the area surrounding dLGN, no other thalamic nuclei receive RGC input. Fluorescence near the top of the image indicates axons of passage, en route to superior colliculus. White line indicates the outline of the dLGN as defined by the Allen Brain Atlas. Yellow box outlines the area plotted in panel C.
F. Relationship between pupil size and $DRN^{5HT \rightarrow dLGN}$ stimulation. F_1: Mean change in pupil size (normalized to the maximal pupil size during each recording session) during $DRN^{5HT \rightarrow dLGN}$ optogenetic stimulation. Black circles indicate the mean across trials for each mouse (n = 6). We did not observe consistent changes in pupil diameter evoked by local stimulation of $DRN^{5HT \rightarrow dLGN}$ axons, in contrast to previous studies that activated all DRN serotonin neurons (Cazettes et al., 2021; Oikonomou et al., 2019). p = 0.99, two-tailed t-test. F_2: Pearson's correlation coefficient for each mouse (n = 6) estimating across-trial covariation between amplitude of $DRN^{5HT \rightarrow dLGN}$ stimulation-evoked suppression of activity at baseline vs. pupil area (pupil area measured in the 2 s preceding onset of optogenetic stimulation). We observed only a weak positive correlation (larger pupil leading to larger amplitude of suppression), indicating that $DRN^{5HT \rightarrow dLGN}$ axon stimulation is not strongly influenced by arousal.
G. Response of individual boutons across single trials during 10 s of $DRN^{5HT \rightarrow dLGN}$ stimulation at baseline (no visual stimulus). Colored dots indicate the ROIs in Fig. 2D and F. Red shaded area at the top indicates time of optogenetic stimulation.
H. Position of RGC boutons across our imaging FOV in superficial dLGN for each mouse, colored by the fractional change in fluorescence ($\Delta F/F$) during stimulation of $DRN^{5HT \rightarrow dLGN}$ axons at baseline.
I. Mean suppression by $DRN^{5HT \rightarrow dLGN}$ optostim at baseline (averaged across boutons) as a function of a bouton's location along the A-P (I_1) and M-L (I_2) axis of dLGN, for each mouse. I_1: anterior is 0 μm, posterior is 800 μm. I_2: medial is 0 μm, lateral is 600 μm.

Figure S3

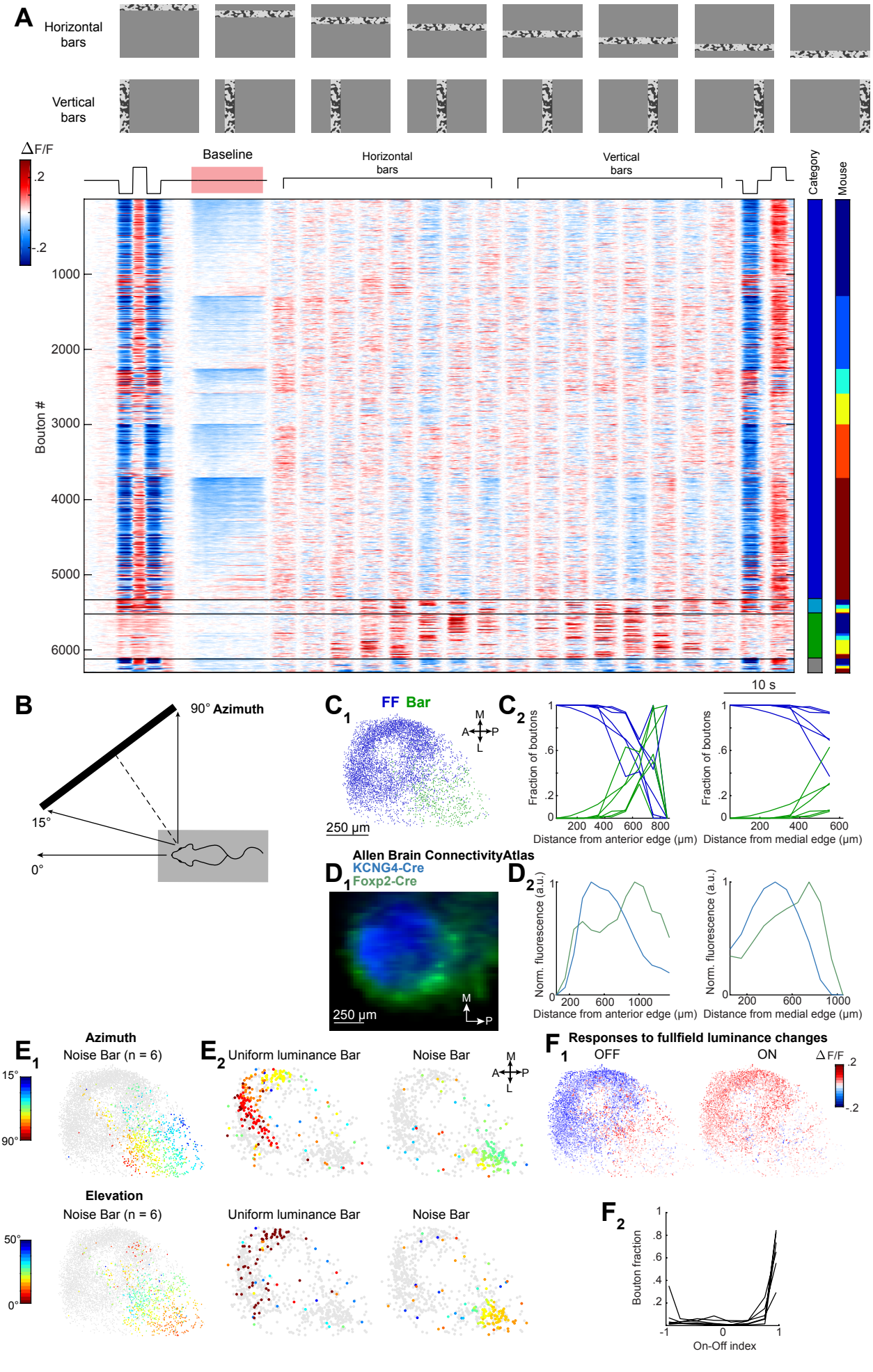
A
Horizontal bars
Vertical bars
ΔF/F
.2
-.2
Baseline
Horizontal bars
Vertical bars
Category
Mouse
Bouton #
1000
2000
3000
4000
5000
6000
10 s
B
90° Azimuth
15°
0°
C1
FF Bar
M
A
P
L
250 µm
C2
Fraction of boutons
Distance from anterior edge (µm)
Distance from medial edge (µm)
Allen Brain ConnectivityAtlas
D1
KCNG4-Cre
Foxp2-Cre
250 µm
D2
Norm. fluorescence (a.u.)
Distance from anterior edge (µm)
Distance from medial edge (µm)
E1
Azimuth
Noise Bar (n = 6)
15°
90°
E2
Uniform luminance Bar
Noise Bar
Elevation
Noise Bar (n = 6)
50°
0°
Uniform luminance Bar
Noise Bar
F1
Responses to fullfield luminance changes
OFF
ON
ΔF/F
F2
Bouton fraction
On-Off index

Figure S3, Detailed analysis of response properties in all driven RGC boutons from two-photon calcium imaging of large fields-of-view in dLGN. Related to Figure 3.

A. *Top*: bars containing binarized white-noise presented horizontally at 8 locations from top to bottom of the screen (50° to 0° in elevation), and vertically at 8 locations from nasal to temporal (15° to 70° in azimuth). *Bottom*: heatmap of mean concatenated responses of boutons from four functional categories (indicated in the colorbar at right; blue/light blue/green/gray indicate FF, FF+bar, Bar and SBC categories, respectively), displayed for all stimulus protocols (6299 boutons from 6 mice, with mouse ID indicated in right-most colorbar). Boutons within each category for each mouse are sorted by mouse ID and then by amplitude of suppression during DRN stimulation at baseline.
B. Diagram showing the position of the monitor and the area of visual space it covers with respect to the mouse during two-photon imaging.
C. *Left* (C_1): spatial distribution, across our imaging FOV in superficial dLGN, of FF and Bar boutons. *Right* (C_2): fraction of boutons in each mouse (individual lines) classified as FF or Bar along the A-P and M-L axes of each FOV. In all of our mice, FF boutons are prevalent in the anterior and medial area of dLGN, whereas Bar boutons are prevalent in the posterior and lateral area.
D. Analysis of data from the Allen Mouse Brain Connectivity Atlas (see also Fig S2C-E). Projection pattern of RGCs of different mouse lines labeled using injection of a Cre-dependent fluorescent marker in one eye. The 3D atlas of the dLGN was tilted (a tilt in pitch [7°] and roll [21°] was applied to match the angle of the imaging window) and re-sectioned to mimic the view through the cannula during two-photon imaging. *Left* (D_1): view of the dorsolateral dLGN, with overlay of inputs from alpha-RGCs (blue; Kcng4-Cre) and from F RGCs (green; Foxp2-Cre). *Right* (D_2): quantification of the intensity of Kcng4-Cre and Foxp2-Cre axons along the A-P and M-L axes in the image in D_1. We observed a similar pattern of spatial segregation of the axons from these two RGC families as for FF vs. Bar axonal boutons (panel C). These apparent differences in innervation by functionally distinct cell types suggests that the most posterior end of our FOV likely sampled from the lower edge of the dLGN 'shell' (a subregion of dLGN which extends more ventrally in the posterior dLGN, Kerschensteiner and Guido (2017)), while the more anterior portion of our FOV may graze the dorsal edge of the dLGN 'core' (in part due to the tilt in pitch of our imaging window).
E. *Left* (E_1): retinotopic organization of RGC boutons across the FOV, aligned and combined across all 6 mice (1 FOV per mouse). Each bouton is colored by its preferred retinotopic location in elevation (bottom) and azimuth (top). Note that retinotopic preference was only estimated for boutons responding robustly (using the quality index described in Methods) to binarized white-noise bars. *Right* (E_2): retinotopic organization in an example mouse in which retinotopy was estimated using both binarized white-noise bars (right panels) and uniformly bright or dark bars (left panels; using the mean unsigned reponse amplitude to dark and bright bars, see Methods). Only driven boutons are shown. Note that distinct sets of boutons display retinotopic preference to these two stimuli: driven boutons in anterior dLGN (the area enriched for FF boutons) respond to bars of uniform luminance, and driven boutons in posterior dLGN (the area enriched for Bar boutons) respond to white-noise bars. Scalebar: 0° in azimuth represents the region of the visual field directly in front of the mouse (see Fig S3B), 0° in elevation is level with the eye. This shows that FF boutons do have retinotopic tuning and are strongly driven by uniform bars, but not white noise bars. Note that in the example FOV, the boutons responding to uniform bars have receptive fields near the bottom of the monitor.
F. *Top* (F_1): response amplitude (fractional change in fluorescence, $\Delta F/F$) of each bouton to a fullfield luminance increment (ON) and to a fullfield luminance decrement (OFF). Note that boutons in the posterior dLGN had strikingly lower response amplitude to fullfield luminance stimuli. *Bottom* (F_2): distribution of On-Off preference index for each mouse (n = 6). Note that On-Off preference index was only estimated for boutons responding robustly (using quality index described in Methods) to fullfield luminance changes.

Figure S4

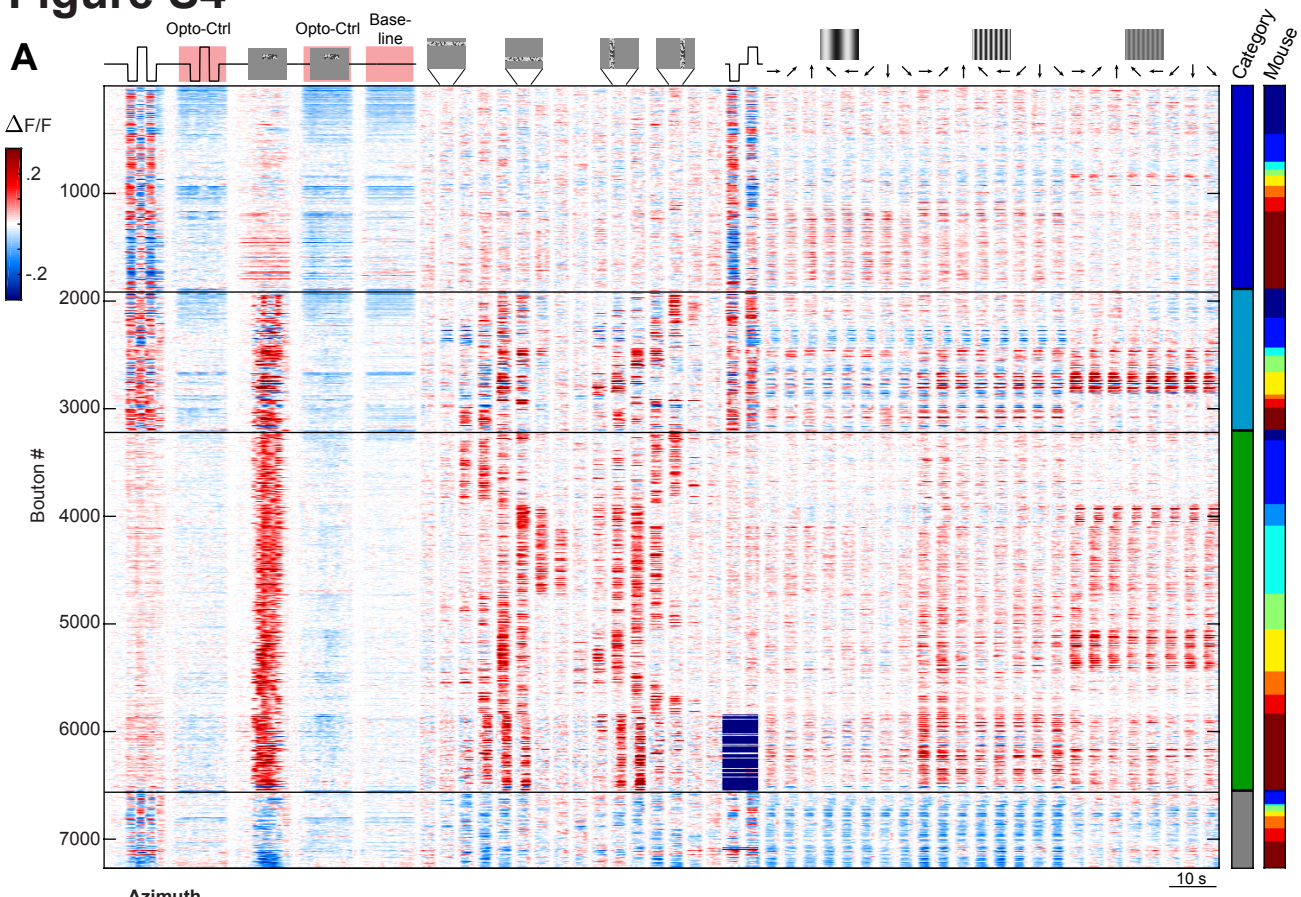
A
Opto-Ctrl
Opto-Ctrl
Base-line
Category
Mouse
ΔF/F
.2
-.2
Bouton #
1000
2000
3000
4000
5000
6000
7000
10 s

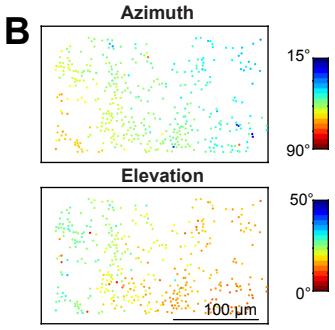
B
Azimuth
15°
90°
Elevation
50°
0°
100 μm

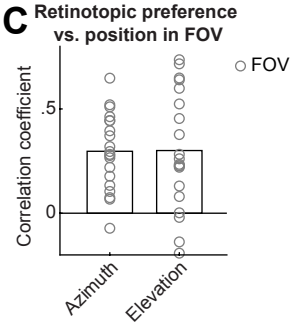
C
Retinotopic preference vs. position in FOV
FOV
Correlation coefficient
.5
0
Azimuth
Elevation

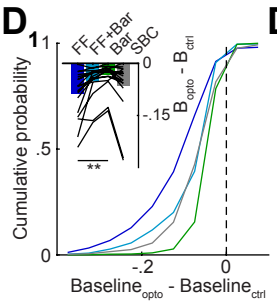
D1
Cumulative probability
1
.5
0
FF
FF+Bar
Bar
SBC
0
-.15
Bopto - Bctrl
**
-.2
0
Baselineopto - Baselinectrl

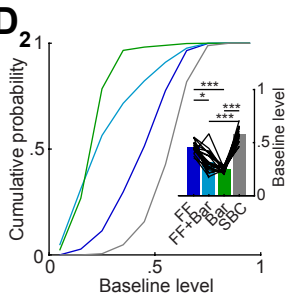
D2
Cumulative probability
1
.5
0
***
*
***
***
1
.5
0
Baseline level
FF
FF+Bar
Bar
SBC
0
.5
1
Baseline level

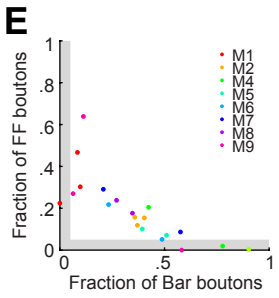
E
Fraction of FF boutons
1
.8
.6
.4
.2
0
M1
M2
M4
M5
M6
M7
M8
M9
0
.5
1
Fraction of Bar boutons

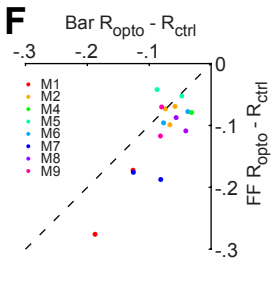
F
Bar Ropto - Rctrl
-.3
-.2
-.1
0
M1
M2
M4
M5
M6
M7
M8
M9
FF Ropto - Rctrl
-.1
-.2
-.3

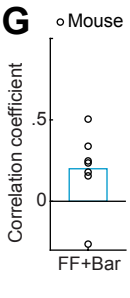
G
Mouse
Correlation coefficient
.5
0
FF+Bar

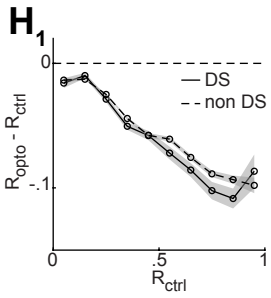
H1
0
-.1
Ropto - Rctrl
DS
non DS
0
.5
1
Rctrl

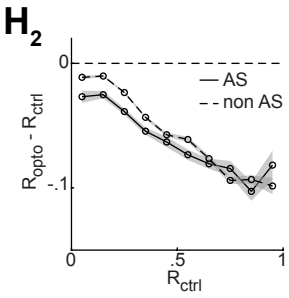
H2
0
-.1
Ropto - Rctrl
AS
non AS
0
.5
1
Rctrl

Figure S4, Detailed analysis of response properties in all driven RGC boutons from two-photon calcium imaging of high-magnification fields-of-view in posterior dLGN. Related to Figure 4.

A. Heatmap of mean concatenated responses of boutons from four functional categories (indicated in the colorbar at right; blue/light blue/green/gray indicate FF, FF+bar, Bar and SBC categories, respectively), displayed for all stimulus protocols. Boutons within each category are sorted first by mouse ID, and then by amplitude of suppression by $DRN^{5HT \rightarrow dLGN}$ stimulation compared to control trials, for time points for which the bouton's activity was between 0.5 and 0.7 of their dynamic range on control trials (7270 boutons from 20 FOV in 9 mice). We only included those boutons that were driven at levels between 0.5 and 0.7 of their dynamic range on control trials of either of the two stimuli that were also paired with optogenetic stimulation – specifically, a 6-s stepwise luminance change and a 6-s sequence of small bars containing white-noise, each presented for 1 s, see Movie S2 and Methods). Mouse ID for each bouton is indicated in the right-most colorbar, across all mice imaged in analyses related to Figure 4 (n = 9).
B. Example FOV showing retinotopic organization. Dots indicate bouton positions, colored by preferred retinotopic location along the azimuth (estimated using elongated vertical bars containing white noise presented at 8 locations on the screen, see top of panel A) and the elevation (defined by horizontal elongated bars containing white noise presented at 8 locations on the screen, see top of panel A). Scale bar: 0° in azimuth represents the front of the mouse (see Fig. S3B), 0° in elevation is level with the eye. See also Fig. S3E for comparison with retinotopy in the low-magnification FOV of the whole dorsal surface of dLGN.
C. Mean correlation coefficient for boutons in each FOV between their position along the A-P axis and their preferred retinotopic location in azimuth (*left bar*), and their position along the M-L axis and their preferred retinotopic location in elevation (*right bar*). Both show a positive correlation, indicating that boutons in each FOV are spatially organized according to their retinotopic preference (more posterior boutons prefer stimuli in more ventral visual field, more lateral boutons prefer stimuli in more temporal visual field).
D. *Left* (D_1): Cumulative distributions of difference in baseline (baseline activity on opto trials [B_{Opto}] – baseline activity on ctrl trials [B_{Ctrl}], each normalized to dynamic range) during $DRN^{5HT \rightarrow dLGN}$ stimulation for the four categories of RGC boutons. LME: all distributions were significantly suppressed, $p < .001$ (except Bar, $p < .05$); all distributions were significantly different from each other: $p < .001$. Inset: mean per FOV (black lines, n = 20) and across FOV (bars). Distributions of means of each FOV were significantly different for FF vs. Bar boutons (Kruskal-Wallis test with post hoc Dunn's multiple comparison test, **$p < .01$). *Right* (D_2): Cumulative distributions of mean activity during baseline (normalized to dynamic range). Inset: mean per FOV (black lines, n = 20) and across FOV (bars). FOV means for FF vs. Bar, FF+bar vs. SBC, and SBC vs. Bar: ***$p < .001$, for FF vs. FF+bar: * $p < .05$ (Kruskal-Wallis with post hoc Dunn's).
E. Fraction of Bar and FF boutons in each FOV. M1-M9 indicate Mouse #1-9. For FOV and mouse analyses, only those FOVs were included for which > 5% of boutons of each category were present (gray shaded areas indicate areas resulting in excluded FOVs based on these criteria).
F. Mean suppression during $DRN^{5HT \rightarrow dLGN}$ stimulation, averaged across time points at which activity was between 0.5 and 0.7 of the dynamic range on control trials, for FF and Bar boutons. Each dot indicates a FOV (n = 16), colors indicate individual animals (n = 8). The stronger stimulation–evoked suppression of FF boutons was consistent across FOVs and mice.
G. Correlation coefficient between $DRN^{5HT \rightarrow dLGN}$ stimulation-evoked suppression and spatial frequency preference. The correlation was computed across all FF+bar boutons that were also driven by drifting gratings. Dots represent the correlation coefficient for each mouse. In 6/7 mice, boutons that preferred lower spatial frequencies were more suppressed by $DRN^{5HT \rightarrow dLGN}$ stimulation (indicated by a positive coefficient). See also Figure 4G and raw data in Figure S4A for FF+bar boutons (indicated by light blue in colorbar at right).
H. Mean suppression due to optostim (R_{opto} - R_{ctrl}) across boutons separated based on direction selectivity index (H_1, DS boutons have DSI > .4) and axis selectivity index (H_2, AS boutons have ASI > .4 and DSI < .4). Only boutons are included with robust responses to drifting gratings. Lines: mean +/- SEM across boutons.

Figure S5

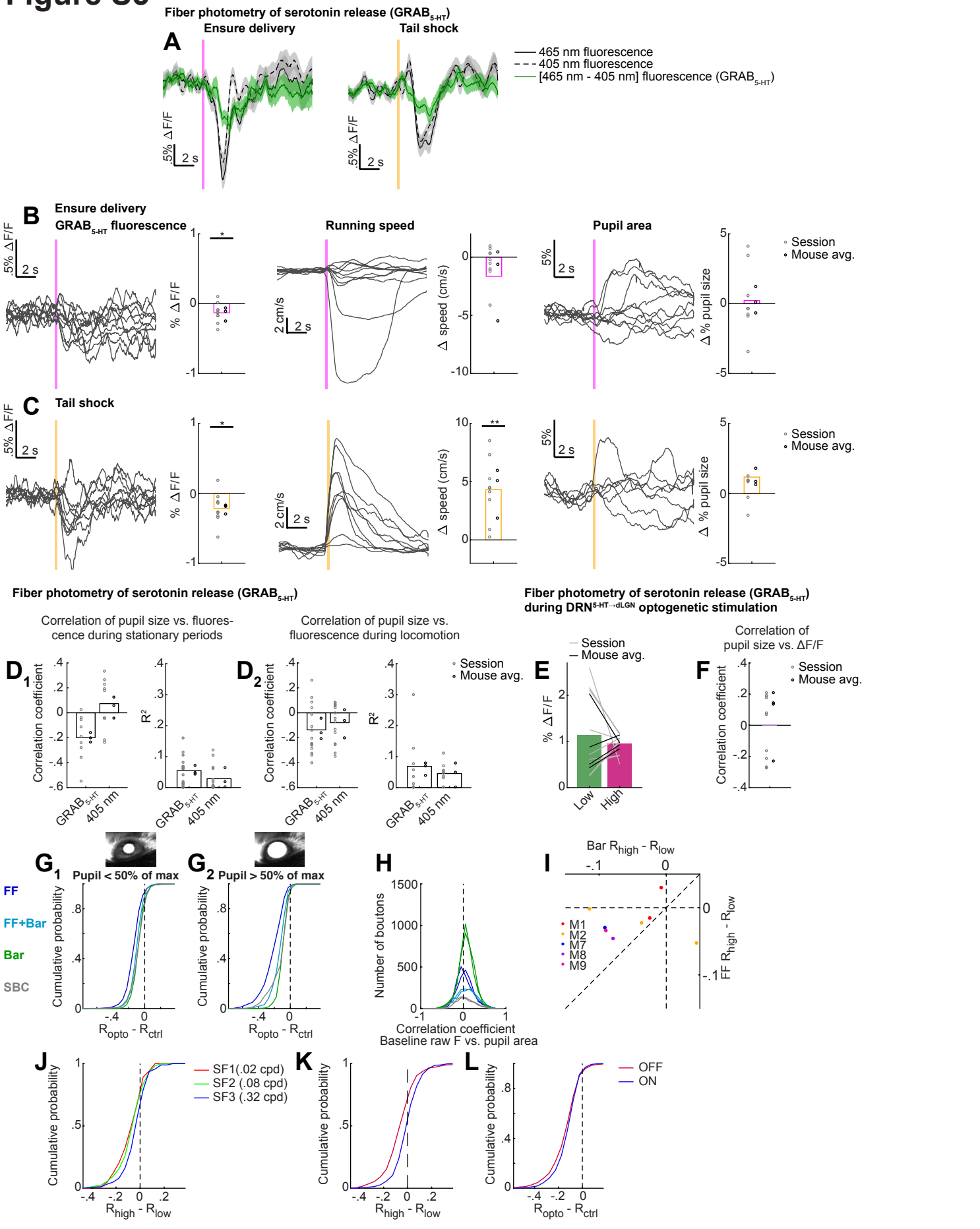
Fiber photometry of serotonin release (GRAB5-HT)
A
Ensure delivery
Tail shock
465 nm fluorescence
405 nm fluorescence
[465 nm - 405 nm] fluorescence (GRAB5-HT)
5% ΔF/F
2 s
B
Ensure delivery
GRAB5-HT fluorescence
Running speed
Pupil area
% ΔF/F
2 cm/s
Δ speed (cm/s)
5%
Δ % pupil size
Session
Mouse avg.
C
Tail shock
Fiber photometry of serotonin release (GRAB5-HT)
Correlation of pupil size vs. fluorescence during stationary periods
Correlation of pupil size vs. fluorescence during locomotion
D1
D2
Correlation coefficient
R2
GRAB5-HT
405 nm
Fiber photometry of serotonin release (GRAB5-HT) during DRN5-HT→dLGN optogenetic stimulation
E
% ΔF/F
Low
High
Correlation of pupil size vs. ΔF/F
F
G1
Pupil < 50% of max
G2
Pupil > 50% of max
FF
FF+Bar
Bar
SBC
Cumulative probability
Ropto - Rctrl
H
Number of boutons
Correlation coefficient
Baseline raw F vs. pupil area
I
Bar Rhigh - Rlow
FF Rhigh - Rlow
M1
M2
M7
M8
M9
J
SF1(.02 cpd)
SF2 (.08 cpd)
SF3 (.32 cpd)
Rhigh - Rlow
K
L
OFF
ON

Figure S5, Serotonin release in dLGN is weakly inversely correlated with arousal. Related to Figure 5.

A. Example mean changes in $GRAB_{5\text{-}HT}$ fluorescence collected at 465 nm and 405 nm in an awake head-fixed mouse, during tail shocks (orange bar) and delivery of single drops of Ensure milkshake (pink bar, mean +/- SEM across trials). 405 nm excitation is near the isosbestic point for this sensor (~425 nm), and thus fluorescence traces at this wavelength are a useful control for brain motion or other artifactual signals, as fluorescence excited by 405 nm light is not sensitive to changes in serotonin. The 405 nm trace for the whole recording session was scaled and subtracted from the 465 nm trace for the whole recording session to correct for motion artifacts (see Methods). The mean response in the resulting subtracted trace (465 nm – 405 nm; termed the 'GRAB' trace) is also shown. All GRAB traces shown and used in Figure S1D-E, 5B-D, S5B-D are the difference between fluorescence traces with excitation at 465 nm and 405 nm. F_0 used to calculate $\Delta F/ F_0$ for each trace is calculated using the 5 s before Ensure or tail shock delivery as F_0.
B. Mean changes in $GRAB_{5\text{-}HT}$ fluorescence, pupil area and running behavior in response to Ensure delivery (pink bar). The traces are mean traces for each session (10 sessions (9 sessions for pupil), 3 mice), the bar plots are the mean amplitude across sessions (amplitude measured as the mean change from 2-4 s after the delivery of Ensure). Gray dots: sessions. Black dots: mice. * $p < .05$.
C. Mean changes in $GRAB_{5\text{-}HT}$ fluorescence, pupil area and running behavior in response to tail shock (orange bar). The traces are mean traces for each session (9 sessions [7 sessions for pupil], 3 mice), the bar plots are the mean amplitude across sessions (amplitude measured as the mean change from 2-4 s after the delivery of Ensure). Grey dots: sessions. Black dots: mice. ** $p < .01$; * $p < .05$.
D. *Left column of each panel:* correlation between pupil area and $GRAB_{5\text{-}HT}$ fluorescence (465 nm – 405 nm fluorescence; negative correlation coefficient: pupil area is inversely correlated with fluorescence). *Right column of each panel:* correlation between pupil area and fluorescence recorded at 405 nm excitation. D_1: pearson's correlation coefficients and R^2 for the linear regression restricted to stationary periods, D_2: pearson's correlation coefficients and R^2 for the linear regression restricted to non-stationary periods. $GRAB_{5\text{-}HT}$ fluorescence is weakly negatively correlated with arousal, even though pupil area explains little variance in $GRAB_{5\text{-}HT}$ fluorescence. During non-stationary periods, 405 nm fluorescence is also weakly negatively correlated, indicating that motion might contribute to the findings for $GRAB_{5\text{-}HT}$ fluorescence. However, when restricting analyses to stationary periods, $GRAB_{5\text{-}HT}$ fluorescence is still weakly negatively correlated with arousal, whereas 405 nm fluorescence is not, confirming that the negative correlation between $GRAB_{5\text{-}HT}$ fluorescence and pupil area is not due to motion artifacts.
E. Mean change in $GRAB_{5\text{-}HT}$ fluorescence on Opto trials, separated by arousal state. High arousal trials were defined as mean pupil area > 50% of maximal area in the 2 s preceding optogenetic stimulation. Low arousal trials were defined as mean pupil area < 50% of maximal area in the 2 s preceding optogenetic stimulation (9 sessions [gray lines], 4 mice [black lines]). Linear mixed effects model (LME): $p = .89$.
F. Correlation coefficient estimating across-trial covariation between arousal state (i.e. mean pupil area in the 2 s preceding optogenetic stimulation) and the amplitude of the change in $GRAB_{5\text{-}HT}$ fluorescence from 2 s before to 2-4 s after optogenetic stimulation (10 sessions [gray dots], 4 mice [black dots]). Positive correlation coefficient: pupil area is correlated with fractional change in GRAB fluorescence. 0/10 coefficients were significant.
G. *Bottom left*, G_1: cumulative distribution of optostim-evoked suppression ($R_{Opto} – R_{Ctrl}$), for time points when each bouton's activity was within 0.5-0.7 of its dynamic range on Ctrl trials, restricted to trials with pupil size <50% of maximal pupil size in a given recording session. LME: all distributions were significantly suppressed, $p < .001$; FF vs. Bar, FF vs. FF+Bar, SBC vs. FF $p<.001$, SBC vs. FF+Bar $p<.01$. *Bottom right*, G_2: cumulative distribution of optostim-evoked suppression ($R_{Opto} – R_{Ctrl}$), for time points when each bouton's activity was within 0.5-0.7 of its dynamic range on Ctrl trials, restricted to trials with pupil size >50% of maximal pupil size in a given recording session. LME: all distributions were significantly suppressed, $p < .001$; FF vs. Bar, FF vs. FF+Bar, SBC vs. FF, $p<.001$, SBC vs. FF+Bar $p<.05$. *Top left and right*: median pupil size for trials used in lower plots.
H. Distribution of correlation coefficients for across-trial correlation between raw fluorescence (F) at baseline (before trial onset) and pupil size, for boutons of each category (positive correlation coefficient: large pupil area is correlated with high baseline raw fluorescence). While this analysis did not correct for bleaching (to avoid associated confounds such as under- or over-fitting), the correlation coefficients were estimated separately on the first and second half of the recording session, indicated by the two lines of each color. Both estimates yielded similar results, suggesting that the results were not the result of clustering of high or low arousal trials at the start or end of the session. The similar lack of correlation for all categories indicates that

differences in arousal modulation across types are not due to baseline suppression (e.g. FF boutons are not suppressed by arousal during visual stimulus presentation, nor at baseline).

I. Mean suppression by arousal (analyzed using timepoints in which the activity on control trials was between 0.5 and 0.7 of the bouton's dynamic range) for FF and Bar boutons in each FOV. FOVs were only included if they had at least 5 trials each at both high and low arousal (defined as higher or lower than 50% of maximum pupil size). Each dot indicates a FOV (n = 8), colors indicate individual mice (n = 5). The stronger arousal-evoked suppression of Bar boutons was consistent across FOVs. Note that, while our previous study (Liang et al., 2020) characterized arousal modulation in RGC boutons in posterior dLGN that were robustly driven by gratings, the arousal modulation of FF boutons had not been directly addressed.

J. Cumulative distributions of R_{high} - R_{low} of FF+Bar boutons with different spatial frequency preferences. R_{high} - R_{low} was calculated for time points when each bouton's activity was between .5-.7 of its dynamic range. LME: distributions for SF1 (.02 cpd) and SF2 (.08 cpd), but not SF3 (.32 cpd) preferring boutons were significantly suppressed, $p < .001$. SF1 vs. SF3, $p < .01$; SF2 vs. SF3, $p < .001$. SF1: 83, SF2: 470, SF3: 184 boutons (10 FOV, 6 mice).

K. Cumulative distributions of R_{high} - R_{low} of FF and FF+Bar boutons separated into ON or OFF types (based on their preference for increases or decreases in luminance, respectively; see Methods). R_{high} - R_{low} was calculated for time points when each bouton's activity was between .5-.7 of its dynamic range on control trials. LME: OFF (but not ON) boutons were significantly suppressed, $p < .001$; ON vs. OFF distribution, $p < .001$. ON: 358, OFF: 477 boutons (10 FOV, 6 mice).

L. Cumulative distributions of $R_{opto} – R_{ctrl}$ of FF and FF+Bar boutons separated into ON or OFF types (based on their preference for increases or decreases in luminance, see Methods). $R_{opto} – R_{ctrl}$ was calculated for time points when each bouton's activity was between .5-.7 of its dynamic range on control trials. LME: OFF and ON boutons were significantly suppressed, $p < .001$; ON vs. OFF distribution, $p < .001$. ON: 916, OFF: 817 boutons (19 FOV, 9 mice).

Figure S6

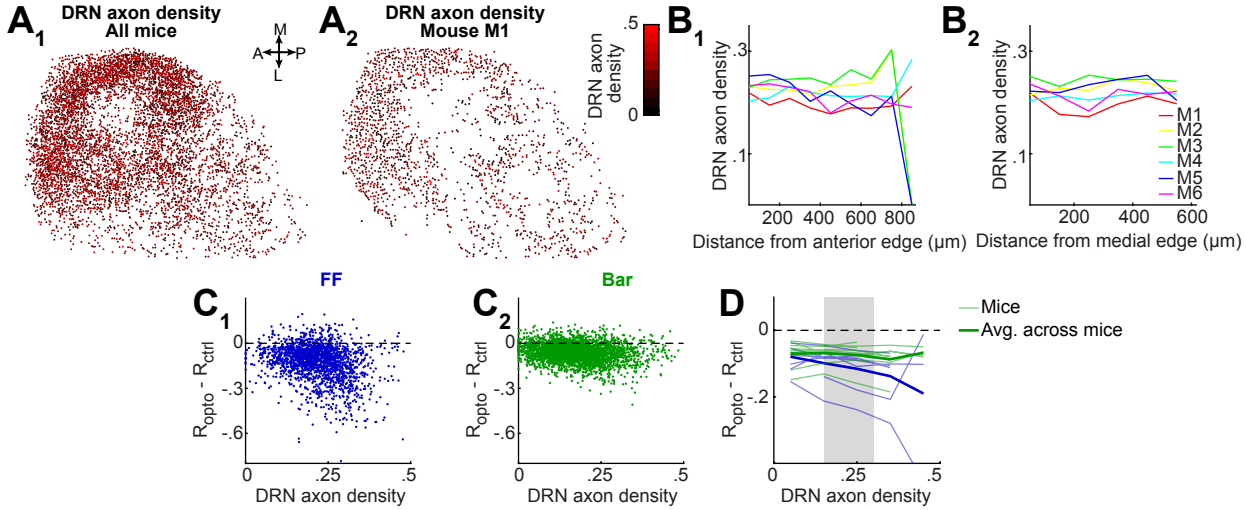
A1
DRN axon density
All mice
M
A
P
L
A2
DRN axon density
Mouse M1
DRN axon density
.5
0
B1
DRN axon density
.3
.1
200 400 600 800
Distance from anterior edge (μm)
B2
DRN axon density
.3
.1
200 400 600
Distance from medial edge (μm)
M1
M2
M3
M4
M5
M6
C1
FF
Ropto - Rctrl
0
-.3
-.6
0 .25 .5
DRN axon density
C2
Bar
Ropto - Rctrl
0
-.3
-.6
0 .25 .5
DRN axon density
D
Ropto - Rctrl
0
-.2
0 .25 .5
DRN axon density
Mice
Avg. across mice

Figure S6, Further analyses of DRN axon density in dLGN. Related to Figure 6.

A. Spatial distribution of local DRN axon density across low-magnification FOVs from all mice (aligned to a common template as in Figure S3C$_1$). Dots represent bouton centroid locations in each FOV, colored using the fraction of pixels belonging to DRN axons in a 10 μm disk surrounding the bouton's center of mass (0 = no pixels, 1 = all pixels in the 10 μm disk belong to DRN axons; see Methods). A$_1$: all boutons from all mice (n = 6), after alignment of FOV based on the morphology of GCaMP expression pattern (see Methods, Figure S2A); A$_2$: boutons from example mouse in Figure 6A.
B. Mean across all boutons in each mouse of the local DRN axon density along the A-P (B$_1$) and M-L (B$_2$) axes, showing no large-scale differences in DRN axon density around boutons as a function of location along the dorsolateral surface of dLGN.
C. Suppression of baseline activity by DRN$^{5HT\rightarrow dLGN}$ stimulation as a function of local DRN axon density, for FF (C$_1$) and Bar (C$_2$) boutons.
D. Mean suppression by DRN$^{5HT\rightarrow dLGN}$ stimulation at baseline as a function of local DRN axon density, plotted separately across FF boutons and Bar boutons in each mouse. Thin lines: mean per mouse (9 mice), thick line: mean across mice.

Figure S7

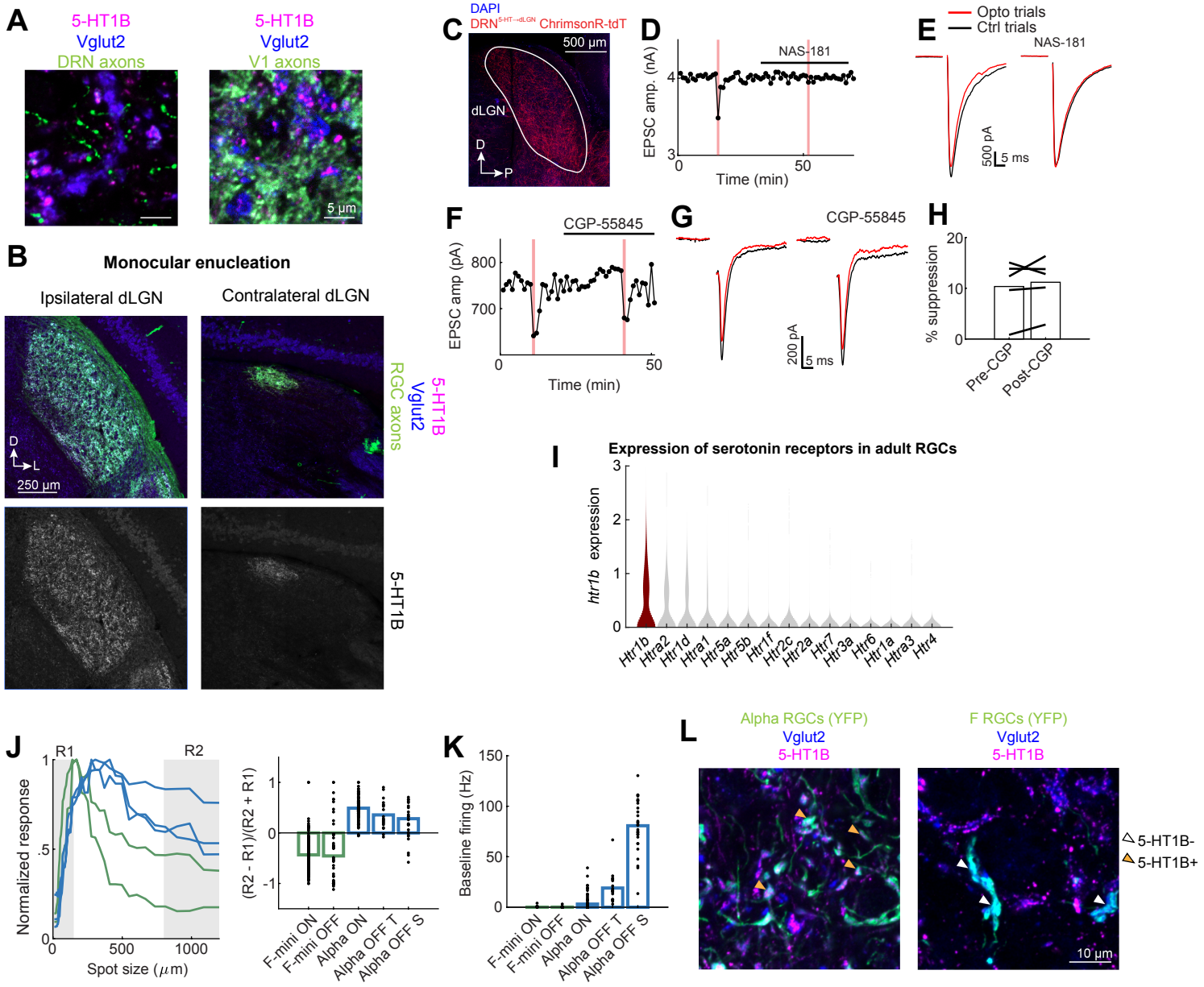
A
5-HT1B
Vglut2
DRN axons
5-HT1B
Vglut2
V1 axons
5 µm
B
Monocular enucleation
Ipsilateral dLGN
Contralateral dLGN
D
L
250 µm
5-HT1B
Vglut2
RGC axons
5-HT1B
C
DAPI
DRN 5-HT→dLGN ChrimsonR-tdT
500 µm
dLGN
D
P
D
NAS-181
EPSC amp. (nA)
Time (min)
E
Opto trials
Ctrl trials
NAS-181
500 pA
5 ms
F
CGP-55845
EPSC amp (pA)
Time (min)
G
CGP-55845
200 pA
5 ms
H
% suppression
Pre-CGP
Post-CGP
I
Expression of serotonin receptors in adult RGCs
htr1b expression
Htr1b
Htra2
Htr1d
Htra1
Htr5a
Htr5b
Htr1f
Htr2c
Htr2a
Htr7
Htr3a
Htr6
Htr1a
Htra3
Htr4
J
R1
R2
Normalized response
Spot size (µm)
(R2 - R1)/(R2 + R1)
F-mini ON
F-mini OFF
Alpha ON
Alpha OFF T
Alpha OFF S
K
Baseline firing (Hz)
F-mini ON
F-mini OFF
Alpha ON
Alpha OFF T
Alpha OFF S
L
Alpha RGCs (YFP)
Vglut2
5-HT1B
F RGCs (YFP)
Vglut2
5-HT1B
10 µm
5-HT1B-
5-HT1B+

Figure S7, $DRN^{5HT \rightarrow dLGN}$ stimulation-evoked suppression of glutamate release from RGCs is not mediated by $GABA_B$ receptors; additional evidence that 5-HT1B is localized to specific sets of RGC boutons. Related to Figure 7.

A. Immunohistochemistry of 5-HT1B (magenta) and Vglut2 (blue) in a coronal slice of dLGN expressing YFP in DRN axons (green, left, Pet1-Cre; FLEX-ChR2-YFP) or in V1 corticothalamic axons (green, right; labeled by injection of fluorescent marker in V1, see Methods).
B. Immunohistochemistry of 5-HT1B (magenta) and Vglut2 (blue) in a coronal slice of dLGN expressing YFP in RGC axons (green, Chx10-Cre; FLEX-ChR2-YFP) after monocular enucleation. The dLGN contralateral to enucleation shows a loss of YFP+ RGC axons, as well as Vglut2 and 5-HT1B expression (only inputs to the 'ipsilateral patch' remain). The ipsilateral dLGN shows intact innervation from the remaining eye.
C. TdTomato expression illustrates DRN innervation in a parasagittal slice of dLGN, used for whole-cell recording of thalamocortical cells.
D. Example recording showing EPSC amplitudes over consecutive trials prior to and following bath application of a 5-HT1B receptor antagonist (NAS-181, 10 μM). Red bars indicate trials for which electrical stimulation of RGC axons was paired with optogenetic stimulation of DRN axons.
E. Left: single traces of EPSCs from the recording in D during a single optogenetic stimulation trial and the mean over the five preceding control trials. Right: same as left but after bath application of NAS-181. Electrical stimulus artifacts were blanked for clarity.
F. Example time course of the peak EPSC amplitude recorded at -70 mV over consecutive trials before and during bath application of a $GABA_B$ receptor antagonist (CGP-55845, 2 μM). Red bars indicate trials for which electrical stimulation of RGC axons was paired with optogenetic stimulation of DRN axons.
G. Left: single traces of EPSCs from the recording in F during an optogenetic stimulation trial and the mean over the three preceding control trials. Right: same as on the left but after bath application of $GABA_B$ receptor antagonist, CGP-55845. Electrical stimulus artifacts were blanked for clarity.
H. Mean percent suppression across all recorded thalamocortical neurons, before and after bath application of CGP-55845. Lines: individual neurons (n = 5). P = .4701, two-tailed paired t-test.
I. Violin plot of the expression of all serotonin receptors (in log [Transcripts Per Million, TPM]) in all RGCs (35,699 cells). This plot is an analysis of a publicly available dataset of adult RGC single cell sequencing (Tran et al., 2019).
J-K. Analysis of publicly available data from rgctypes.org involving whole-cell electrophysiology recordings in whole mount retina.
J. Receptive field properties of two types of F-mini RGCs (green, F-mini ON and F-mini OFF) and three types of alpha RGCs (blue, ON alpha, OFF sustained alpha and OFF transient alpha). Left: peak-normalized mean firing rate in response to focal illumination of the retina with discs of increasing radius. Shaded areas indicate spots with diameter >800 μm and <150 μm. Right: mean preference index for responses to large spots (>800 μm [~26° of visual space], R2) vs. small spots (<150 μm [~5° of visual space], R1), calculated as (R2-R1)/(R2+R1). Dots indicate individual recorded cells (F-mini ON: n = 197; F-mini OFF: n = 69; ON alpha: n = 98; OFF Sustained alpha: n = 30; OFF Transient alpha; n = 20).
K. Baseline firing (in darkness) of two F-mini RGC types (green) and three alpha RGC types (blue).
L. Example histology of F-mini RGC axons (green; labeled with YFP using Foxp2-Cre mice; ~75% of Cre-expressing RGCs are F-mini) or alpha RGC axons (green; labeled with YFP using Kcng4-Cre; >90% of Cre-expressing RGCs are alpha RGCs), co-stained with Vglut2 (blue) and 5-HT1B (magenta). Orange and white arrowheads indicate YFP+ boutons with or without 5-HT1B co-expression, respectively.